ICRH induced particle losses in Wendelstein 7-X

J.M. Faustin[1], W.A. Cooper[1], J.P. Graves[1], D. Pfefferlé[1] and J. Geiger[2]

[1]Ecole Polytechnique Fédérale de Lausanne (EPFL), Swiss Plasma Center (SPC), CH-1015 Lausanne, Switzerland

[2]Max-Planck Institut für Plasmaphysik, D-17491 Greifswald, Germany

Abstract

Fast ions in W7-X will be produced either by Neutral Beam Injection (NBI) or by Ion Cyclotron Resonant Heating (ICRH). The latter presents the advantage of depositing power locally and does not suffer from core accessibility issues [M. Drevlak et al *Nucl. Fusion* 2014]. This work assesses the possibility of using ICRH as a fast ion source in W7-X relevant conditions. The SCENIC package is used to resolve the full wave propagation and absorption in a three-dimensional plasma equilibrium. The source of the Ion Cyclotron Range of Frequency (ICRF) wave is modelled in this work by an antenna formulation allowing its localisation in both the poloidal and toroidal directions. The actual antenna dimension and localization is therefore approximated with good agreement. The local wave deposition breaks the five-fold periodicity of W7-X. It appears that generation of fast ions is hindered by high collisionality and significant particle losses. The particle trapping mechanism induced by ICRH is found to enhance drift induced losses caused by the finite orbit width of trapped particles. The inclusion of a neoclassically resolved radial electric field is also investigated and shows a significant reduction of particle losses.

1 Introduction

The large superconductor stellarator Wendelstein 7-X (W7-X) has recently obtained its first plasma at IPP-Greifswald, Germany. This first quasi-isodynamic stellarator ever built is expected, amongst other achievements, to demonstrate satisfactory confinement of fast ions. The confinement of fusion-born alpha particles is of primary concern for fusion reactors because they represent a substantial source of plasma heating. The optimisation procedure which resulted in the design of W7-X has provided the possibility of obtaining not only good fast particles confinement but also equilibrium and stability properties compatible with safe operation at high $\langle\beta\rangle$ value, i.e. up to 5%. The experimental success of W7-X relies in part on the generation of fast ions (typically hydrogen) within 50keV to 100keV, which are comparable to alpha particles in a reactor in terms of Larmor radius to machine minor radius ratio. Generation of such fast ions is hindered by many effects which must be understood in the context 3D fields.

As exposed in Ref. [1], the quasi-isodynamic design would be best suited for a stellarator fusion reactor because it should be in principle capable of confining alpha particles over their slowing-down time. Studies into fast particle losses have broadened the understanding of the complicated dynamics of these particles in stellarators. The class of orbits that particles can take in a particular stellarator field [2, 3] has been found to have a strong impact on their confinement properties. It was found in Ref. [4] that the confinement of trapped particles relies mainly on the magnetic field structure and particularly on the geodesic curvature of the magnetic field lines. A process of collisionless stochastic radial diffusion acting on transitioning (or blocked) fast ions was first introduced in Ref. [1] and exposed with more details in Ref. [5]. Fast particle losses due to more exotic orbits, e.g. stochastic trapped orbits, were thoroughly studied in Refs. [6, 7]. The confinement of fast ions in various W7-X configurations were published in Ref. [8]. The behaviour of a fast ion population generated by neutral beam injection (NBI) was investigated at $\langle\beta\rangle = 2\%$ and showed issues regarding the beam penetration and also rapid loss of injected particles. It was also suggested in this work that using Ion-Cyclotron Resonant Heating (ICRH) would constitute a suitable alternative to NBI for fast ion generation mainly because ICRH does not suffer from the same core accessibility issues. ICRH is expected to be able to deposit power and therefore generate fast ions directly in the plasma centre where equilibrium confinement properties have to be tested

experimentally. In the present paper, the possibility of producing fast ions using a minority ICRH scheme in W7-X is addressed. The SCENIC code package [9,10] is used in order to solve for the W7-X plasma equilibrium, the fast wave propagating in the Ion-Cyclotron Range of Frequency (ICRF) and the interaction of minority ions with the ICRF wave along their guiding-centre trajectories. The analysis of the resulting ICRH particle distribution function provides an understanding particle losses mechanisms and fast ion confinement that leads to the generation of tails associated with ICRF heating. It is shown that the fraction of fast particles is significantly lower than the one produced in a similar tokamak scenario. The lost particle fraction is also found to be significantly high.

This paper is organised as follows. SCENIC simulations resolving consistent particle distribution functions in W7-X plasmas, where a minority ICRH scheme is applied, are presented in section 2. The main loss channels acting on fast ions in W7-X configurations exposed in Ref. [11] are briefly described in section 3. The lost particle distribution is then discussed in section 4. In section 5, the effect of a radial electric field provided by neoclassical transport calculations on the ICRH distribution function is investigated.

2 SCENIC simulations

2.1 Equilibria

The set of modular and planar coils which forms the W7-X magnetic system possesses the capacity to explore various magnetic configurations defined by the mirror ratio parameter [8,12]:

$$mr = \frac{B_{\varphi=0} - B_{\varphi=\pi/5}}{B_{\varphi=0} + B_{\varphi=\pi/5}}, \tag{1}$$

where $B_{\varphi=0}$ is defined at the bean shaped cross section.

The VMEC/ANIMEC code [13,14] was used in order to reconstruct a high-mirror ($mr = 8.7\%$) and a standard ($mr = 4\%$) equilibrium. These configurations were chosen in order to emphasize the issues related to ICRF wave propagation and absorption under particular equilibrium magnetic field toroidal variation. In particular, the amplitude of the toroidal gradient in the magnetic field amplitude can be such that the lowest $|B|$ value in the bean shaped cross section is higher than the highest $|B|$ value in the triangular cross section. Therefore, as seen in Fig. 1 for the high-mirror configuration, there is no particular $|B|$ value present at all toroidal positions. The consequence of this is that no ICRH frequency can be chosen such that a resonance will be found inside the plasma at all toroidal angles.

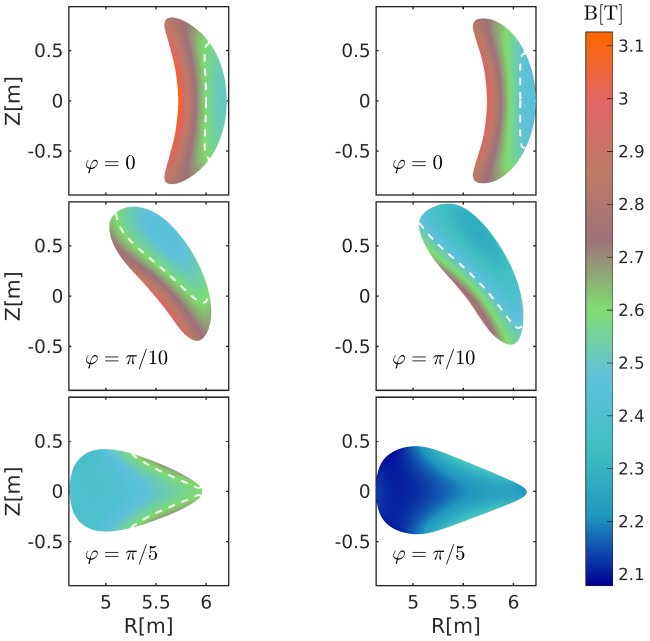

Figure 1 – Poloidal cross sections of W7-X equilibria used (left: standard configuration, right: high-mirror configuration). Colors indicate the amplitude of the equilibrium magnetic field. Dashed white lines show the location of the fundamental H resonance corresponding to 39.6MHz (left) and 38.1MHz (right) respectively.

2.2 Wave field calculation

The 3D full wave code LEMan [15, 16] computes the ICRF wave propagation based on a prescribed ICRF antenna excitation. The calculation of the dielectric tensor $\hat{\epsilon}$is based on the warm plasma model and resolves only electron Landau damping and fundamental ion cyclotron resonance. In the presence of a hot particle population which can be approximated by a bi-Maxwellian model, the dielectric tensor is corrected accordingly. Therefore only wave-particle interaction at the fundamental frequency on the minority species is possible. The LEMan code solves the Maxwell's equations in terms of vector and scalar potentials (resp. $\mathbf{A}$ and $\tilde{\phi}$) under the Coulomb Gauge choice $\nabla \cdot \mathbf{A} = 0$):

$$\nabla^2 \mathbf{A} + k_0^2 \hat{\epsilon} \cdot \mathbf{A} + ik_0 \hat{\epsilon} \cdot \tilde{\phi} = -\frac{4\pi}{c} \mathbf{j}_{ant} \tag{2}$$

$$\nabla \cdot \left(\hat{\epsilon} \cdot \nabla \tilde{\phi}\right) - ik_0 \nabla \cdot (\hat{\epsilon} \cdot \mathbf{A}) = -4\pi \rho_{ant} \tag{3}$$

The source for the fast magneto-sonic wave modeled in LEMan, is given by the current density $\mathbf{j}_{ant}$ flowing in the ICRF antenna straps [17]. In tokamak plasmas the poloidal modes of the fast wave are strongly coupled because of the inherent poloidal asymmetry of the equilibrium. This coupling is taken into account by the introduction of a poloidally localised simulated antenna.

These plasmas can be approximated to be axisymmetric allowing an only weak coupling between the toroidal modes of the fast wave. It is therefore valid to consider each toroidal mode of the excitation spectrum independently from one another. Each of these modes can be computed by letting the antenna surround the plasma in the toroidal direction. The wave localisation is retrieved by a superposition of a chosen set of modes which dominate the antenna spectrum. However this procedure is no longer valid in a 3D equilibrium because the asymmetry found also in the toroidal direction imposes a coupling of the fast wave toroidal modes. The modeled antenna in LEMan can take into account this additional coupling by localising the antenna in both the poloidal and toroidal direction. This is performed in the LEMan code by a particular implementation of the current density $\mathbf{j}_{ant}$ in the RHS of eq. (2). The general expression for $\mathbf{j}_{ant}$ is written by considering no charge accumulation in the antenna and takes the following divergence-free form in the straight field line Boozer coordinate system (s, θ, φ) [15]:

$$\mathbf{j}_{ant} = \nabla s \times \nabla \sigma(s, \theta, \varphi) \tag{4}$$

In eq. (4), $\sigma(s, \theta, \varphi)$ is a function describing the localisation and the extension of the antenna excitation and reads :

$$\sigma\left(s, \theta, \varphi\right) = \sigma_s\left(s\right) \sigma_\theta\left(\theta\right) \sigma_\varphi\left(\varphi\right) \tag{5}$$

$$= \prod_{X=s,\theta,\varphi} (1 - X^2)^2 \mathcal{B}\left(\frac{X - X_1}{X_1 - X_2}\right) \tag{6}$$

In eq. (6), $s_{1,2}$, $\theta_{1,2}$, $\varphi_{1,2}$ define the antenna spatial boundaries and $\mathcal{B}$ is the box function which equals 1 in the interval $[-1; 1]$ and 0 elsewhere. The flux coordinate frame in which the whole SCENIC suite of codes is written limits the simulated plasma domain to span from the magnetic axis to the last closed flux surface (LCFS). Therefore the antenna excitation cannot be radially positioned in the vacuum region but it is instead cast into a radial domain within the last closed surface. The complicated physics describing the plasma-wave coupling that occurs between the LCFS and the antenna can therefore not be modeled and a perfect coupling is assumed. The W7-X ICRF antenna system to be installed for operation phase (OP) 1.2 is described in Ref. [18] and is used to set the modeled current density to a realistic configuration. This excitation model is applied to solve for the fast wave deposition in a W7-X Deuterium rich plasma with 0.5% Hydrogen minority. The central density and temperature were respectively set to $n_0 = 1.55 \times 10^{20} m^{-3}$ and $T_0 = 4.5 keV$ for the standard equilibrium and $n_0 = 1.5 \times 10^{20} m^{-3}$ and $T_0 = 4 keV$ for the high-mirror configuration. These values of density and temperature were chosen in order to ensure a converged equilibrium with $\langle\beta\rangle \simeq 4\%$ for each configuration. The excitation frequency was respectively set to 38.1MHz and 39.6MHz for the high-mirror and standard mirror cases. The right-handed wave electric field amplitude around the midplane is displayed in Fig. 2. As previously described in ref. [19],

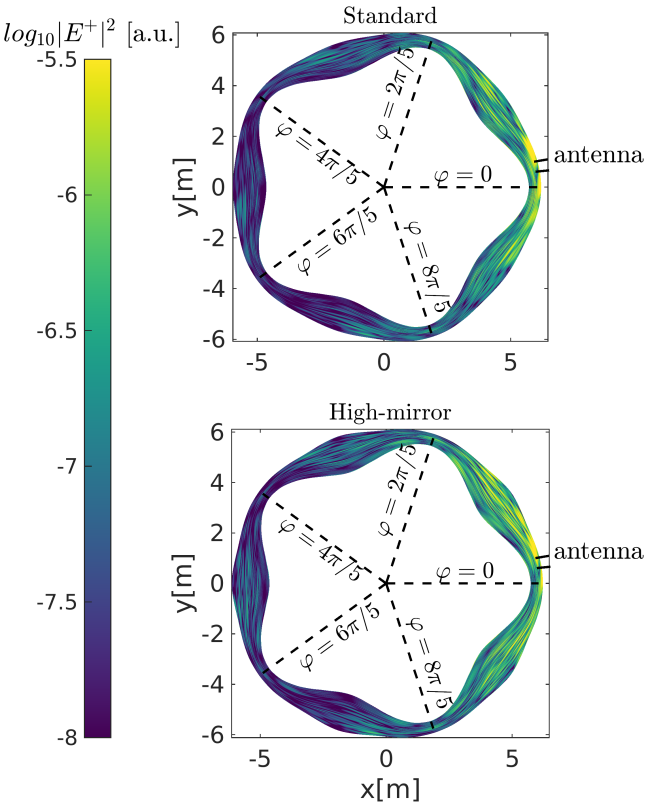

Figure 2 – Right-handed electric field amplitude distribution (log scale) around the midplane [a.u.] for the standard (top) and the high-mirror (bottom) W7-X configuration.

the localisation of the antenna excitation is seen in the toroidal dependency of the electric field. The modeled antenna is located in the toroidal period spanning the domain $\varphi = [0, 2\pi/5]$ and is the locus of the highest electric field amplitude. The other toroidal periods are more distant to the excitation source and display reduced electric field amplitude. The five-fold symmetry breaking is explained by considering the damping of the wave as it travels toroidally and crosses the resonant layers. Fig. 2 also illustrates the effect of the magnetic configuration on the wave propagation. As mentioned in section 2.1, the resonance layer disappears from the confined plasma volume in certain regions of the high-mirror configuration. Therefore the wave is not absorbed continuously as it propagates toroidally

and its amplitude is maintained.

2.3 Guiding centre orbit calculations

The VENUS-LEVIS code [20] is used to resolve the guiding centre orbits of the H minority ions. Monte Carlo operators [21] are implemented in order to compute the Coulomb collisions with the thermal ions and electrons and the ICRF wave-particle interaction [22]. The electric field and wave numbers computed by the LEMan code with the localised antenna modeled is used for the latter. The simulated ICRF power is set to 1.5MW which corresponds to a realistic power under the assumption of perfect antenna-plasma coupling. The energy transfer to and from the minority ions is in particular investigated. It is important to state that the wave energy is considered to be absorbed uniquely by the minority species. However, given the minority concentration used (0.5%) and the choice of the plasma ion species, a non negligible fraction of the power is expected to be absorbed by the Deuterium ions by second harmonic wave-particle interaction. As mentioned earlier, it is not our intention to provide fully realistic ICRH scenario simulations but instead the principle of generating and confining a fast particle population with ICRH in a high density stellarator plasma is investigated. A thermal population of $2'097'152$ H markers is initialised in both equilibria. The minimum energy for the marker initialisation was set to 1keV because only the behaviour of supra-thermal particles are of interest in this work. These markers are evolved for a time equivalent to a fourth of a slowing down time. The resulting energy distribution functions are displayed in Fig. 3. A case that has been obtained from a SCENIC simulation of a JET plasma run for a fourth o a slowing down time with 1.5MW power is also shown comparison. As described in [22], a splitting of the tail and the

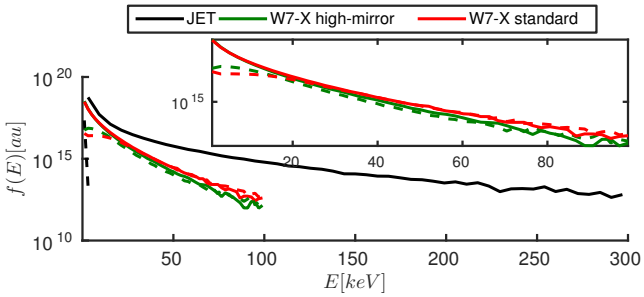

Figure 3 – Distribution function in energy of confined vs lost minority ions for the two investigated W7-X configurations compared with a JET case. Dashed lines show the lost particle energy distribution, which for the JET case is seen to be negligible and comparable to the confined particles for the W7-X cases.

components of the final distribution can be performed in minority ICRH scenarios. In typical SCENIC simulations, the hot component of the particle distribution is fitted to the bi-Maxwellian model described in Ref. [23] and the corresponding moments are then used to update the plasma equilibrium and the ICRF wave deposition consistently with the hot particles contribution [22]. Several iterations between the 3 components of the SCENIC package allows the computation of a self-consistent distribution function. However, the fast

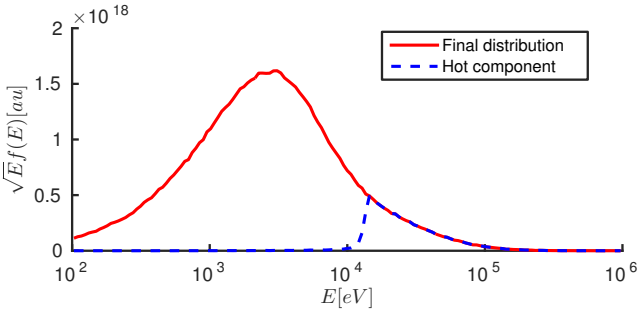

Figure 4 – ICRH distribution and its corresponding hot component obtained from a JET equilibrium.

component of the distributions for the W7-X cases of Fig. 3 are nearly vanishing. This can mainly be explained by the high density considered in these simulations. It is known from [24] and [25] that the minority energy range scales like $1/n_e^2$. The SCENIC iteration scheme cannot straightforwardly be applied using the usual procedure applied for tokamaks, but the particle distribution can still be analysed. Moreover, it is seen in Fig. 3 that the distribution of lost particles, i.e. particles which cross the LCFS, represents a significant fraction of the initial distribution: $\sim 12\%$ of the markers are lost during those simulations. The markers have the same numerical weight, therefore the fraction of lost markers represents the same number of lost particles. The amount of losses in a similar scenario applied to an axisymmetric JET tokamak plasma is nearly vanishing mainly because of the symmetry of trapped particle orbits in such a configuration. Note that changing the equilibrium from a standard to a high-mirror configuration seems only to affect the wave deposition pattern as seen in Fig. 2. Indeed, the change in the fast ion tail and the lost particle distribution appears to be negligible. Therefore, the analysis of the loss channels under ICRH conditions carried out in the next section, focuses on the high-mirror configuration. It will be seen later however that the losses can be reduced significantly by including neoclassically resolved electric fields.

3 Loss channels

Loss channels acting on a fast particle population generated by NBI were presented in [11]. In summary the losses are associated with the class of orbit which the particles are following.

Stochastic radial diffusion. This mechanism affects the transitioning particles, which are locally trapped in a toroidal period but can de-trap collisionlessly. This diffusion was suggested in Ref. [1] and further developed in Ref. [5]. This process acts on fast particles and is rather slow in the sense that a particle needs to experience several collisionless transitions between the locally trapped and passing state before it diffuses radially. In these simulations however, the initial distribution contains predominantly thermalised, i.e. collisional particles from which a fast tail would be generated. Therefore this mechanism is not expected to play a significant role in the formation of the lost particles distribution.

Drift induced losses. Particles bouncing in the main magnetic mirrors or local magnetic wells can experience a net radial drift depending on the local properties of the equilibrium. The bounce averaged radial drift can be written in terms of the geodesic component of the magnetic field line curvature, assuming MHD force balance and nested flux surfaces:

$$\oint_{bounce} \boldsymbol{v_D} \cdot \frac{\nabla s}{|\nabla s|} \mathrm{d}t = \oint_{bounce} -\left(\frac{\mu}{q} + v_{\parallel}\rho_{\parallel}\right) \frac{B}{B^*_{\parallel}} \kappa_g \mathrm{d}t, \tag{7}$$

$$\kappa_g = \frac{1}{\sqrt{g}B^2\sqrt{g^{ss}}} \left(\frac{\partial B}{\partial \theta} B_{\varphi} - \frac{\partial B}{\partial \varphi} B_{\theta}\right). \tag{8}$$

where a particle of charge q, mass m and magnetic moment μ is considered, and $\rho_{\parallel} = mv_{\parallel}/qB$, $B^*_{\parallel} = \boldsymbol{B}/B \cdot \left(\boldsymbol{B} + \rho_{\parallel}\nabla \times \boldsymbol{B}\right)$. The magnetic flux coordinate system is defined ($s = \Phi_{tor}/\Phi_{tor,edge}, \theta, \varphi$) and the corresponding Jacobian is $\sqrt{g} = (\nabla s \times \nabla\theta \cdot \nabla\varphi)^{-1}$. It follows from eq. (7) that heated particles must avoid being localised in regions where the geodesic curvature is negative in order to reduce the particle losses.

Effects of collisions. In addition to collisional transport, pitch-angle scattering may cause particles to wander in and out the trapped-passing boundary. It was shown in Ref. [11] that this process can populate regions of phase space where particles are deeply trapped in local wells with predominant unfavourable geodesic curvature.

Effects of ICRH. The ICRF acceleration results in a net increase of the resonant particles energy and magnetic moment after crossing multiple times the resonant layer. It is recalled that for trapped particles, the amplitude of the ambient magnetic field for which the parallel velocity vanishes is given by:

$$B_{ref} = \frac{E}{\mu} = B\left(1 + \frac{v_{\parallel}^2}{v_{\perp}^2}\right) \tag{9}$$

After the wave-particle interaction, a resonant particle's perpendicular and parallel velocities are modified as:

$$v_{||,\perp} \rightarrow v_{||,\perp} + \Delta v_{||,\perp} \tag{10}$$

The ICRF wave-particle interaction occurs predominantly in the direction perpendicular to the magnetic field, so that after many interactions, in eq. (10): $\Delta_{net} v_{\perp} \gg \Delta_{net} v_{||}$. Inspection of eq. (9) under this condition shows that the net energy transfer from the wave to the particle decreases its B_{ref} value until $B_{ref} = B_c = m\omega_{ant}/q$, where ω_{ant} is the wave frequency provided by the antenna excitation. Therefore the ICRF wave is a source of particle trapping and hence in typical 3D configurations, ICRH resonance leads to an enhancement of the drift induced losses. Most of these loss channels described in this section are observed in the VENUS-LEVIS simulations presented in Section 4.

4 Lost particle distribution analysis

The most significant loss channels introduced in Section 3 act predominantly on trapped particles. Figure 5 correlates the amount of lost markers for a given pitch angle variable $1/B_{ref} = \mu/E$. In this figure, the vertical dotted lines locate the particular value $1/max\ B|_{\phi=0}$ and $1/min\ B|_{\phi=0}$. These lines give an estimation of the fraction of deeply passing and deeply trapped particles. As suggested in Section 3, pitch angle scattering produced by Coulomb collisions can generate deeply trapped particles which escape the confined volume via the drift induced loss mechanism. This mechanism explain the loss pattern observed when no ICRH is applied (dashed line in Fig. 5). It is seen that the losses practically do not affect passing particles. On the other deeply trapped particles localised around the triangular cross section experience significantly this loss mechanism as seen by the peak in the region $1/Bref > 1/min\ B|_{\phi=0}$. In addition to this effect, the ICRF wave absorption brings resonating particles into a locally trapped state, therefore increasing the fraction of particles experiencing drift induced losses. In Fig. 5, this is illustrated by the first (small) peak in the dash-dotted line. The corresponding B_{ref} value for this peak matches the chosen value of B_c for this simulation. This is caused by the alignment mechanism of the particles bounce tip with the resonant layers described in section 3. Moreover, the choice of B_c, and therefore of the ICRH frequency,

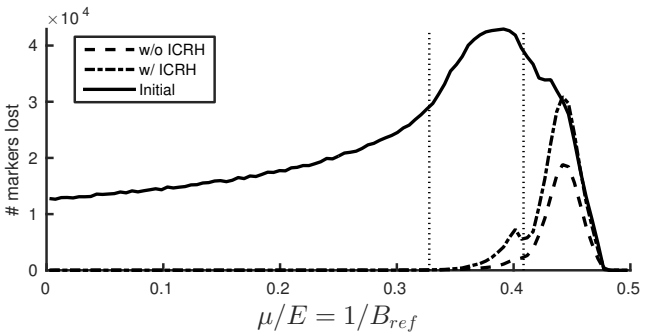

Figure 5 – Number of lost markers as a function of their pitch angle variable μ/E. All markers located to the left (resp. right) of $1/max\ B|_{\phi=0}$ (resp. $1/min\ B|_{\phi=0}$) are deeply passing (resp. trapped). The peak on dash-dotted line at $\mu/E = 0.4$ corresponds to $1/B_c$.

has then a direct impact on the fraction of lost particles. Fig. 6 compares the number of lost markers for different values of B_c, showing significant increases as B_c decreases from $2.5T$ to $2.4T$ and to $2.22T$. As expected from the trapping mechanism described earlier, the largest peak in the number of lost markers is observed at $1/B_{ref} = 1/B_c$.

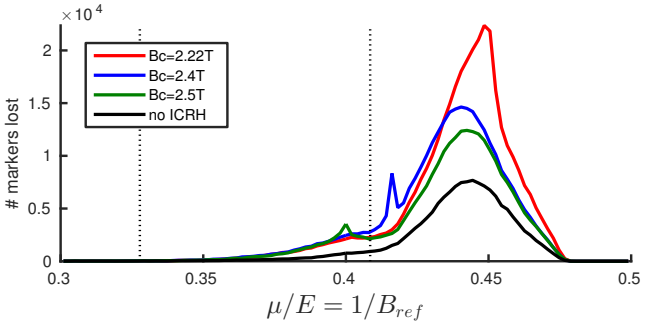

Figure 6 – Number of lost markers as a function of their pitch angle variable μ/E for various ICRH frequencies. The location of peaks corresponding to enhanced particle losses due to ICRH moves from $\mu/E = 0.4$ ($B_c = 2.5T$) to $\mu/E \simeq 0.416$ ($B_c = 2.4T$) and to $\mu/E = 0.45$ ($B_c \simeq 2.22T$)

The change in the ICRH frequency also changes the toroidal region covered by the resonant layer which in turn influences the number of particles in the trapped region of phase-space. Indeed, for lower values of B_c, e.g. $2.22T$, the resonant layers are mostly located around the triangle cross section. In this case, the resonant particles' motion converts into a toroidally trapped state which causes these particles to bounce between two poloidally closed isosurfaces (i.e. that entirely cover the $\theta = [0, 2\pi]$ domain) at $B = B_c = B_{ref}$. These particles can strongly experience the drift induced loss channel described earlier. Locally passing particles are usually well magnetically confined as it has been previously described. On the other hand confining deeply trapped and energetic particles using only the magnetic equilibrium structure is one of the main challenges of the quasi-isodynamic stellarator configuration because their bounce averaged poloidal drift motion, especially at high energies, may not compensate their outward radial drift. As it was mentioned in section 3 where eq. (7) was defined, these deeply trapped particles are lost because their trajectory is mostly located in regions of negative geodesic curvature. On the other hand, higher values of B_c, e.g. $2.5T$, correspond to resonant layers mostly located around the bean-shaped cross section. As seen in Fig. 7, the isosurfaces $B = B_c = B_{ref}$ are poloidally open (isosurfaces that do not span the entire poloidal domain $\theta = [0, 2\pi]$) for $B_c = 2.5T$ at $s = 0.25$. Therefore particles interacting with the ICRF wave are moved towards a helically trapped state, i.e. they can become locally passing by collisionless de-trapping. The drift induced loss mechanism is consequently less efficient for this fraction of trapped particles, this explaining the reduced number of lost markers with increasing value of B_c as observed in Fig. 6.

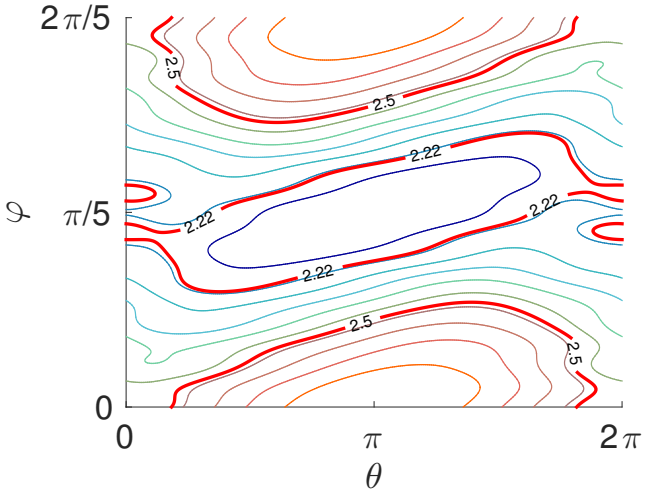

Figure 7 – Contours of constant $|B|$ in the $\theta - \varphi$ plane at $s = 0.25$. The large peaks seen in figs. 5 and 6 correspond to particle trapped between poloidally closed isosurfaces of B (e.g. 2.22T).

The loss patterns are also marked by the wave localisation. It is seen in Fig. 8 that the losses are enhanced in the toroidal period containing the antenna (and to a lesser extent the adjacent one) compared to the losses in the other periods. As expected from the drift induced loss mechanism, particle losses are toroidally localised around local magnetic wells as seen from the black curve

in Fig. 8. It is expected that pitch-angle scattering provided by Coulomb collisions re-distributes particles in phase-space until they eventually trap in a local magnetic well and possibly drift out of the plasma. In addition to this redistribution, ICRH traps particles in particular magnetic wells which corresponds to the chosen frequency, or B_c value. Finally, there is a remarkable asymmetry in the loss patterns observed in each single period (e.g., a peak at the entrance of each period not found at the other end of the period) which was explained in Ref. [11] by the stellarator anti-symmetric feature of the geodesic curvature.

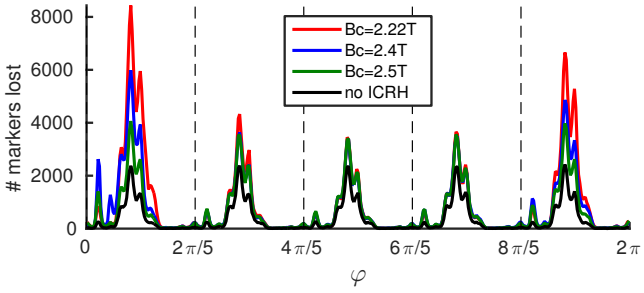

Figure 8 – Number of lost markers with respect to their toroidal position. If the antenna was not localised, the total number of lost markers is expected to be higher than in the work presented here.

5 Guiding centre simulations including a radial electric field

Neoclassical particle transport of background electrons and ions occurs under the ambipolarity condition. The so-called ion-root transport regime [26] gives rise to a radial electric field (E_r) which affects the free motion of charged particles around the magnetic field lines by adding a $\boldsymbol{E} \times \boldsymbol{B}$ drift. The profile used in this work, displayed in Fig. 9, resulted from a neoclassical transport simulation performed with the 1-D transport code NTSS [27]. This calculation was based on a NBI-heated plasma scenario where 5.5MW of NBI-power was absorbed by a rather low density plasma ($8 \times 10^{19} m^{-3}$). The radial electric field profile given by this type of calculation depends on the plasma scenario parameters, e.g. type of heating, plasma density, level of anomalous transport considered. Therefore the E_r-profile displayed in Fig. 9 is not consistent with the ICRH scenario presented in this work. However it can still be used to investigate in principle the effect of the resulting $\boldsymbol{E} \times \boldsymbol{B}$ drift on the ICRH distribution function.

This additional drift component points essentially in the poloidal direction and is expected to improve the

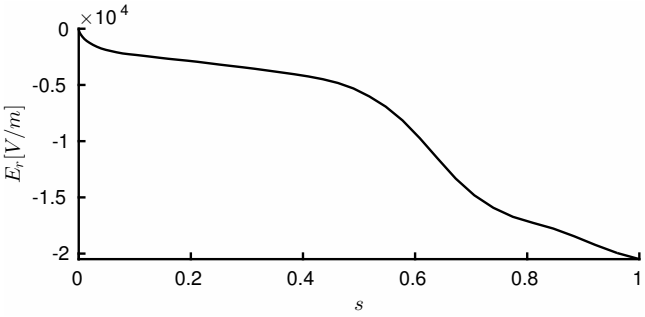

Figure 9 – Radial electric profile E_r resolved by neoclassical calculation.

confinement of trapped particles in non-axisymmetric magnetic configurations. The effects of such an electric field on fast particles were already investigated for an NBI-like population in Ref. [11]. As expected, it was observed that the confining effect of E_r is more efficient at low energies. In this section, the effects of E_r on the distribution function of lost particles and the fast tail generation, are investigated. The guiding centre simulation presented in section 4 with $B_c = 2.5T$ is re-run with the inclusion of E_r. The high equilibrium background density and the relatively low ICRH power dictate that the minority species ions remain mostly thermal and therefore undergo a strong effect of the $\boldsymbol{E} \times \boldsymbol{B}$ drift. In this case undertaken for an ICRH power of $1.5MW$, the number of lost markers is strongly reduced as seen in Fig. 10 and represents a negligible fraction of the initial markers population.

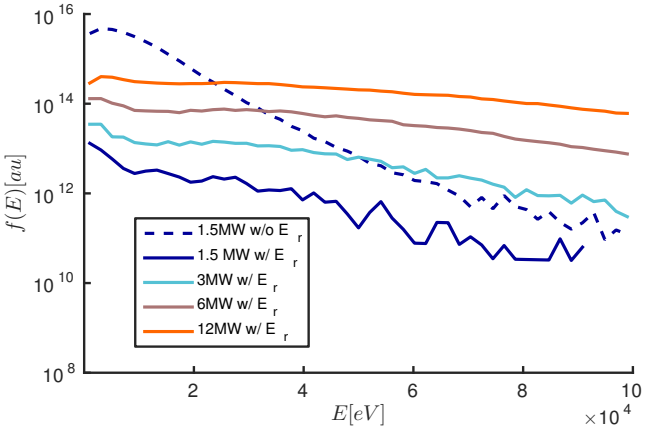

Figure 10 – Distribution functions in energy of lost minority ions with increasing ICRF power in W7-X. The dashed blue case does not include E_r.

The fraction of fast ions in the total minority species distribution function remains relatively low for $1.5MW$. As well known from Ref. [24], the energy range reached by the minority species scales with the coupled ICRF

power P_{RF}. It is seen from Fig. 10 that the particle losses follow roughly the same scaling because higher kicks to the particles' perpendicular velocity increase inevitably the radial drift, see eq. (7). Distribution functions of confined particles resulting from the scan in P_{RF} is shown in Fig. 11. The possibility of generating fast ions at higher heating power is observed for these cases where the radial electric field assists confinement. As P_{RF} increases, the fast ion tail of the distribution grows and becomes similar to the JET-like simulation introduced in section 2.3 for $P_{RF} = 6MW$. However, this amount of coupled power, under the assumption of perfect wave-plasma coupling, is well above the expected maximum available power during OP1.2 [18]. Therefore the minority ICRH scheme does not appear to be suitable for fast ion generation in W7-X.

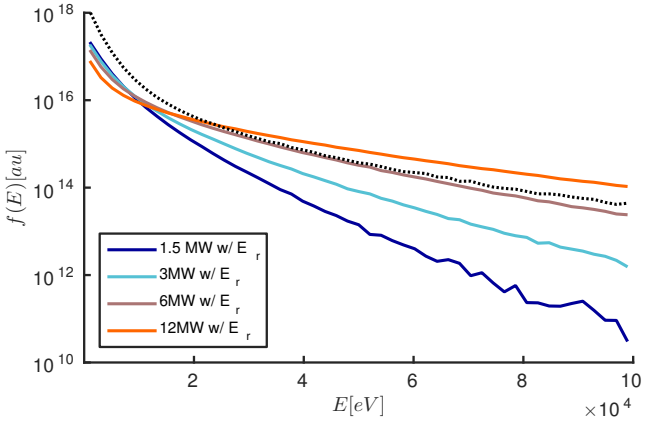

Figure 11 – Distribution functions in energy of confined minority with increasing ICRF power in W7-X. The dotted line shows for comparison the distribution obtained the JET plasma simulation introduced in section 2.3.

6 Summary and conclusions

The work presented here describes the ICRF wave deposition for a minority heating scheme in W7-X and the associated particle losses. Simulations obtained with the 3D full-wave code LEMan show that the localisation of the antenna system induces a five-fold periodicity breaking in terms of wave deposition. This wave field has been used with the guiding centre orbit VENUS-LEVIS in order to resolve the wave-particle interaction. The particle loss patterns characterising the investigated ICRH heated W7-X plasma scenario have been assessed. Particle losses are mostly due to a drift induced loss mechanism. Pitch angle scattering produced by Coulomb collisions is a source of particle trapping and de-trapping and consequently enhances the drift induced losses. ICRH is also found to enhance this loss channel because the wave-particle interaction in the perpendicular direction is a source of particle trapping. Consequently, the toroidal positions of lost particles are influenced by the wave localisation. The effects of a radial electric computed by neoclassical transport simulations have been considered. The inclusion of the $\boldsymbol{v}_{\boldsymbol{E}\times\boldsymbol{B}}$ leads to a more complete description of the particle dynamics and shows a strong reduction of the losses. However, this does not appear to be sufficient for producing a fast ion tail distribution for experimental fast particle confinement studies with 1.5MW of coupled ICRH power. Other ICRH schemes such as the so-called three-ion species heating scenario [25] should be further investigated for the generation of fast ions in W7-X. Regardless of the heating scheme, it seems reasonable that fast ions will be mostly located in the toroidal period containing the antenna and the one adjacent to it because of the RF trapping effect. In addition to the consequences of this on plasma heating in general, the improvements to the ICRH model taking into account such toroidal variation, e.g. in the dielectric tensor, should be considered in the future.

Acknowledgments

The authors would like to thank C. D. Beidler, M. Drevlak, P. Helander, J. Dominski and S. Lanthaler for insightful discussions. The authors are also grateful to D. Moseev and Yu. Turkin for providing the radial electric field profile.

This work has been carried out within the framework of the EUROfusion Consortium and has received funding from the Euratom research and training programme 2014-2018 under grant agreement No 633053. The views and opinions expressed herein do not necessarily reflect those of the European Commission. The project was also supported in part by the Swiss National Science Foundation. The authors thank Dr. S. P. Hirshman for providing us with the VMEC code. Much of the numerical work was performed at the CSCS, Lugano, Switzerland, and at the IFERC, Rokkasho, Japan. This work was supported by EPFL through the use of the facilities of its Scientific IT and Application Support Center.

References

[1] W Lotz, P Merkel, J Nuehrenberg, and E Strumberger. Collisionless alpha -particle confinement in stellarators. *Plasma Phys. Control. Fusion*, 34(6):1037–1052, 1992.

[2] A Gibson and J B Taylor. Single Particle Motion in Toroidal Stellarator Fields. *Phys. Fluids*, 10(12):2653–2659, 1967.

[3] John R. Cary, C. L. Hedrick, and J. S. Tolliver. Orbits in asymmetric toroidal magnetic fields. *Phys. Fluids*, 31(6):1586, 1988.

[4] Horst Wobig. Theory of advanced stellarators. *Plasma Phys. Control. Fusion*, 41(3A):A159–A173, 1999.

[5] C. D. Beidler, Ya. I. Kolesnichenko, V. S. Marchenko, I. N. Sidorenko, and H. Wobig. Stochastic diffusion of energetic ions in optimized stellarators. *Phys. Plasmas*, 8(6):2731, 2001.

[6] M. S. Smirnova. A theory of the helical ripple-induced stochastic behavior of fast toroidal bananas in torsatrons and heliotrons. *Phys. Plasmas*, 8(5 I):1584–1593, 2001.

[7] M. S. Smirnova. Direct losses of fast particles in multiple-toroidicity stellarators. *Phys. Plasmas*, 8(12):5204, 2001.

[8] M. Drevlak, J. Geiger, P. Helander, and Y. Turkin. Fast particle confinement with optimized coil currents in the W7-X stellarator. *Nuclear Fusion*, 54(7):073002, 2014.

[9] M Jucker, J P Graves, W A Cooper, and T Johnson. Ion cyclotron resonance heating with consistent finite orbit widths and anisotropic equilibria. *Plasma Phys. Control. Fusion*, 53(5):054010, May 2011.

[10] M. Jucker, J. P. Graves, W. A. Cooper, N. Mellet, T. Johnson, and S. Brunner. Integrated modeling for ion cyclotron resonant heating in toroidal systems. *Comput. Phys. Commun.*, 182(4):912–925, April 2011.

[11] J M Faustin, W A Cooper, J P Graves, D Pfefferlé, and J Geiger. Fast particle loss channels in Wendelstein 7-X. *submitted to Nuclear Fusion*, 2015.

[12] J Geiger, H Maassberg, and C. D. Beidler. Investigation of Wendelstein 7-X Configurations with Increased Toroidal Mirror. *35th EPS Conference on Plasma Phys. Hersonissos*, 32D:5–8, June 2008.

[13] S. P. Hirshman and J. C. Whitson. Steepest-descent moment method for three-dimensional magnetohydrodynamic equilibria. *Phys. Fluids*, 26(12):3553, 1983.

[14] W. A. Cooper, S. P. Hirshman, P. Merkel, J. P. Graves, J. Kisslinger, H. F G Wobig, Y. Narushima, S. Okamura, and K. Y. Watanabe. Three-dimensional anisotropic pressure free boundary equilibria. *Comput. Phys. Commun.*, 180(9):1524–1533, September 2009.

[15] P. Popovich, W. A. Cooper, and L. Villard. A full-wave solver of the Maxwell's equations in 3D cold plasmas. *Comput. Phys. Commun.*, 175(4):250–263, August 2006.

[16] N. Mellet, W. A. Cooper, P. Popovich, L. Villard, and S. Brunner. Convolution and iterative methods applied to low-frequency waves in 3D warm configurations. *Comput. Phys. Commun.*, 182(3):570–589, March 2011.

[17] R.J. Dumont and D. Zarzoso. Heating and current drive by ion cyclotron waves in the activated phase of iter. *Nuclear Fusion*, 53(1):013002, 2013.

[18] J. Ongena, A. Messiaen, D. Van Eester, B. Schweer, P. Dumortier, F. Durodie, Ye. O. Kazakov, F. Louche, M. Vervier, R. Koch, A. Krivska, A. Lyssoivan, M. Van Schoor, T. Wauters, V. Borsuk, O. Neubauer, O. Schmitz, G. Offermans, Y. Altenburg, C. Baylard, D. Birus, S. Bozhenkov, D. A. Hartmann, J. P. Kallmeyer, S. Renard, R. C. Wolf, and T. Fülöp. Study and design of the ion cyclotron resonance heating system for the stellarator Wendelstein 7-X. *Phys. Plasmas*, 21(6):061514, June 2014.

[19] J. M. Faustin, W. A. Cooper, J. Geiger, J. P. Graves, and D. Pfefferlé. Applications of the SCENIC code package to the minority ion-cyclotron heating in Wendelstein 7-X plasmas. *AIP Conference Proceedings*, 1689(1), 2015.

[20] D. Pfefferlé, W.A. Cooper, J.P. Graves, and C. Misev. Venus-levis and its spline-fourier interpolation of 3d toroidal magnetic field representation for guiding-centre and full-orbit simulations of charged energetic particles. *Computer Physics Communications*, 185(12):3127 – 3140, 2014.

[21] A.H. Boozer and G. Kuo-Petravic. Monte Carlo evaluation of transport coefficients. *Phys. Fluids*, 24(5):851, 1980.

[22] M. Jucker, W.A. Cooper, and J.P. Graves. Integrated modelling of ICRH in a quasi-axisymmetric stellarator. *Nucl. Fusion*, 52(1):013015, January 2011.

[23] W.A Cooper, J.P Graves, S.P Hirshman, T Yamaguchi, Y Narushima, S Okamura, S Sakakibara, C Suzuki, K.Y Watanabe, H Yamada, and K Yamazaki. Anisotropic pressure bi-Maxwellian distribution function model for three-dimensional equilibria. *Nucl. Fusion*, 46(7):683–698, July 2006.

[24] T H Stix. Fast-wave heating of a two-component plasma. *Nuclear Fusion*, 737, 1975.

[25] Ye.O. Kazakov, D. Van Eester, R. Dumont, and J. Ongena. On resonant ICRF absorption in three-ion component plasmas: a new promising tool for fast ion generation. *Nucl. Fusion*, 55:032001, 2015.

[26] P Helander, C D Beidler, T M Bird, M Drevlak, Y Feng, R Hatzky, F Jenko, R Kleiber, J H E Proll, Yu Turkin, and P Xanthopoulos. Stellarator and tokamak plasmas: a comparison. *Plasma Phys. Control. Fusion*, 54(12):124009, December 2012.

[27] Yu. Turkin, H. Maassberg, C. D. Beidler, J. Geiger, and N. B. Marushchenko. Current control by eccd for w7-x. *Fusion Science and Technology*, 50(3):387–394, October 2006.